

Accepted manuscript

Hicheri, R. & Pätzold, M. U. (2021). An RF-Based Positioning Method for Tracing a Cluster of Moving Scatterers in Non-Stationary Indoor Environments. IEEE Wireless Communications Letters, 10(9), 1862-1866. <https://doi.org/10.1109/LWC.2021.3084242>

Published in: IEEE Wireless Communications Letters

DOI: <https://doi.org/10.1109/LWC.2021.3084242>

AURA: <https://hdl.handle.net/11250/3074349>

Copyright: © 2021 IEEE

Available

© 2021 IEEE. Personal use of this material is permitted. Permission from IEEE must be obtained for all other uses, in any current or future media, including reprinting/republishing this material for advertising or promotional purposes, creating new collective works, for resale or redistribution to servers or lists, or reuse of any copyrighted component of this work in other works.

An RF-Based Positioning Method for Tracing a Cluster of Moving Scatterers in Non-Stationary Indoor Environments

Rym Hicheri, *Member, IEEE*, and Matthias Pätzold, *Senior Member, IEEE*

Abstract—This paper presents a novel iterative positioning method for tracing the body segments of a person moving indoors using radio-frequency (RF) signals. The indoor space is equipped with a multiple-input multiple-output (MIMO) communication system. The person is modelled by a cluster of moving point scatterers, playing the role of moving body segments. The proposed technique estimates the time-variant (TV) positions of the moving scatterers by fitting the TV channel transfer function (TVCTF) of the channel model as close as possible to the TVCTF of the measured channels. Numerical results are presented to demonstrate the accuracy of this method.

Index Terms—Indoor propagation, positioning, cluster of scatterers, non-stationary channels, MIMO systems.

I. INTRODUCTION

RADIO-frequency (RF)-based indoor positioning systems (IPSS) find applications in several areas such as medicine, security, surveillance, and robotics [1]. These IPSSs can be classified into two major groups depending on the technique they employ. The first group determines the positions of a moving person by exploiting the received signal strength [2], the time-of-arrival [3], and/or the angle-of-arrival [4]. The second group achieves the positioning task by applying fingerprinting and proximity methods [5], [6].

More papers that summarize and organize recent relevant results can be found in [1], [7], [8]. RF-based IPSSs suffer from severe accuracy degradation due to signal attenuation, multipath propagation, and the strength of the line-of-sight (LOS) path [1], [8]. For example, the impact of the LOS component on the performance of WiFi-based fingerprinting for indoor positioning in non-crowded areas was investigated in [5]. This degradation is especially prominent in uncontrolled environments. Another fact is that all existing positioning methods have been developed for specific settings and thus, their performance is highly dependent on the considered scenario [9]. A review of the literature shows that common assumptions made for existing positioning techniques are linear trajectories [2], [3] and neglecting the fixed objects or/and the non-LOS components [6]. Another common assumption is that the person is not moving for short periods of time [2], [10]. Furthermore, a widely considered assumption is that the human body is modelled by a single point moving scatterer, which represents the centre of the body mass. To the best of our knowledge, existing methods do not allow to trace a cluster of human body segments.

This work was carried out within the scope of the WiCare Project funded by the Research Council of Norway under grant number 261895/F20.

The authors are with the Faculty of Engineering and Science, University of Agder, NO-4898 Grimstad, Norway (email: rym.hicheri@uia.no; matthias.patzold@uia.no).

Manuscript received Nov. 27, 2020; revised Feb. 26, 2021 and April 27, 2021; accepted May 18, 2021.

The motivation of this paper is to overcome the aforementioned limitations by leveraging multiple-input multiple-output (MIMO) configurations to trace a cluster of moving body segments in a three-dimensional (3D) indoor environment. The proposed positioning method was inspired by the iterative non-linear least square approximation (INLSA) algorithm, which was initially introduced in [11]. Owing to the fact that the original INLSA has been developed for estimating the channel parameters of wide-sense stationary (WSS) multipath fading channels, the method cannot be readily applied on estimating the motion curves positions of human body segments in non-WSS indoor channels. The extension of the original INLSA approach to enable the estimation of the time-variant (TV) coordinates of the body segments in non-stationary propagation environments requires to redefine the optimization problem and results in new analytical expressions for estimating the TV channel parameters.

The novelty of this paper is four folds. First, we extend the original INLSA to obtain a new iterative procedure for tracing the different human body segments in indoor environments in the presence of fixed objects and a LOS component. Second, we consider that each body segment plays the role of a moving relay, which is characterized by a radar cross-section parameter. Third, we define a new optimization problem, where the TV positions of the moving scatterers are determined by fitting the TV channel transfer function (CTF) of the non-stationary channel model as close as possible to the TVCTF of the measured radio channels. Fourth, we derive a new exact closed-form solution for the radar cross-section, which reduces drastically the complexity of the underlying optimization problem.

The performance of the proposed estimation method is assessed by comparing the estimated TV positions of the body segments with the corresponding exact (ground truth) TV positions. For a fair comparison, we use test RF signals generated by computer simulations for which the exact TV coordinates of the moving scatterers are known. For a realistic numerical analysis, the TV trajectories of the body segments were extracted by using the musculoskeletal-based OpenSim model [12]. The OpenSim model applies inverse biomechanics and kinematics to describe the dynamics of a system consisting of rigid bodies (bones) and joints upon which forces are acted to produce motion. Moreover, the simulation parameters of the considered orthogonal frequency division multiple access (OFDM) communication system were chosen in accordance with the IEEE 802.11n standard [13]. Numerical results are presented to analyze the impact of noise on the accuracy of the proposed positioning method. Also, a quantitative analysis of the effect of positioning errors on the Doppler characteristic of the channel is performed.

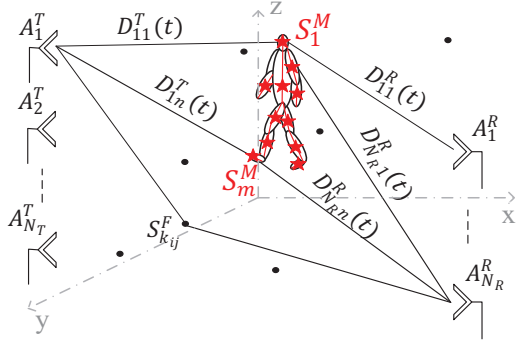


Fig. 1. 3D geometrical model for a non-stationary $N_T \times N_R$ MIMO channel with moving scatterers (★) and fixed scatterers (●).

II. 3D NON-STATIONARY CHANNEL MODEL

A. Scenario Description

In this paper, we consider a scenario which consists of a single person moving in an indoor environment, which contains several fixed objects and is equipped with a distributed $N_T \times N_R$ MIMO system. The transmitter (receiver) T_X (R_X) has N_T (N_R) antenna elements A_j^T (A_i^R). The geometrical channel model describing this multipath propagation scenario is depicted in Fig. 1. The transmit antennas A_j^T ($j = 1, 2, \dots, N_T$) and the receive antennas A_i^R ($i = 1, 2, \dots, N_R$) are located at the fixed positions (x_j^T, y_j^T, z_j^T) and (x_i^R, y_i^R, z_i^R) , respectively. Here, we assume the presence of LOS components. As can be seen in Fig. 1, the moving person is modelled by a synchronized cluster of M moving point scatterers S_m^M ($m = 1, 2, \dots, M$), represented by the symbol (★), which represent the major human body segments. The moving scatterer S_m^M has the TV coordinates $x_m(t)$, $y_m(t)$, and $z_m(t)$, for $m = 1, 2, \dots, M$. We denote by $D_{jm}^T(t)$ ($D_{im}^R(t)$) the TV Euclidean distance between the m th scatterer S_m^M and the j th (i th) transmit (receive) antenna A_j^T (A_i^R). The fixed objects (furniture, walls, decoration items, ...) are modelled by K_{ij} fixed point scatterers $S_{k_{ij}}^F$ ($k_{ij} = 1, 2, \dots, K_{ij}$), which are represented by the symbol (●) in Fig. 1. Single-bounce scattering is assumed when modelling the moving/fixed scatterers.

B. Time-Variant Channel Transfer Function

In reality, the collected RF data is sampled in both the time and frequency domains, where the time sampling interval Δt and the frequency sampling period $\Delta f'$ are known characteristic parameters of the employed channel sounder. The TVCTF $\hat{H}_{ij}(f'_q, t_p)$ of the received RF signal is computed from samples of the measured channel at discrete time instances $t_p = p\Delta t \in [0, T]$ ($p = 0, 1, \dots, P-1$) and discrete frequencies $f'_q = -B/2 + q\Delta f' \in [-B/2, B/2]$ ($q = 0, 1, \dots, Q-1$), where T is the total observation time and B is the frequency bandwidth. Starting from the model depicted in Fig.1, the TVCTF $H_{ij}(f'_q, t_p)$ of the link $A_j^T - A_i^R$ can be obtained as

$$H_{ij}(f'_q, t_p) = \sum_{m=1}^M c_{ijm}(t_p) \exp\left(j\left(\theta_{ijm} - 2\pi(f'_q + f_c)\tau'_{ijm}(t_p)\right)\right) + \sum_{k_{ij}=0}^{K_{ij}} c_{k_{ij}} \exp\left(j\left(\theta_{k_{ij}} - 2\pi(f'_q + f_c)\tau'_{k_{ij}}\right)\right) \quad (1)$$

where f_c is the centre carrier frequency. The first part of

(1) describes the effects of the motion of the cluster of scatterers S_m^M (representing the moving person). As it has been extensively discussed in [14], [15], is a human body is exposed to low-frequency electromagnetic fields, an electric current is induced in the body segments, which in turn behave as moving relays. In this case, the TV path gain $c_{ijm}(t_p)$ of the m th moving scatterer S_m^M is expressed as $c_{ijm}(t_p) = b_m [D_{jm}^T(t_p) D_{im}^R(t_p)]^{-\gamma/2}$. Here, the parameter b_m describes the contribution of the m th scatterer S_m^M , where $\sum_{m=1}^M b_m^2 = 1$. The quantity b_m^2 is known as the radar cross-section [15]. Also, γ is a path loss component dependent on the propagation environment. Common values of γ are between 1.6 and 1.8 in indoor spaces. Moreover, $\tau'_{ijm}(t_p) = [D_{jm}^T(t_p) + D_{im}^R(t_p)]/c_0$ is the TV path delay of S_m^M , where c_0 is the speed of light. The initial phases of the channel θ_{ijm} are modelled by a random variable uniformly distributed over the interval $[0, 2\pi)$.

The second part of (1) describes the multipath propagation resulting from the fixed scatterers. The LOS component does not experience any Doppler effect and can be modelled by a fixed scatterer S_{0ij}^F . The fixed scatterer $S_{k_{ij}}$, $k = 0, 1, \dots, K_{ij}$, are described by constant path gains $c_{k_{ij}}$, constant path delays $\tau'_{k_{ij}}$, and random phase. $\theta_{k_{ij}}$. Here, the phases $\theta_{k_{ij}}$ are uniformly distributed over $[0, 2\pi)$. For simplicity, the second term of (1) is replaced by a single complex term. The validity of non-stationary channel models with TV path gains and TV path delays to describe the channel state information of measured data was confirmed for a single moving point scatterer in [16] and for multiple moving point scatterers in [17], where commercial WiFi devices were used. The measurements were collected in a laboratory room, where activities (e.g., walking, sitting, and falling) were performed.

III. THE PROPOSED ESTIMATION ALGORITHM

The main purpose of this paper is to propose a new iterative procedure to estimate the TV positions $(x_{mp}, y_{mp}, z_{mp}) = (x_m(t_p), y_m(t_p), z_m(t_p))$, $m = 1, 2, \dots, M$, of a cluster of M moving scatterers in a room equipped with a $N_T \times N_R$ communication system, the characteristics of which are assumed to be known. Together with the TV coordinates of the M moving scatterers, the proposed estimation method allows the computation of all channel parameters. Since the fixed scatterers do not experience any Doppler effect, their impact can be removed by applying high-pass filtering.

The problem at hand is to estimate the TV positions $(x_{mp}, y_{mp}, z_{mp}) = (x_m(t_p), y_m(t_p), z_m(t_p))$, the initial phase θ_{ijm} , and the parameters γ and b_m ($m = 1, 2, \dots, M$). To do so, we have to determine, at each time instant t_p , the set of parameters $\mathcal{P}_{t_p} = \{x_{mp}, y_{mp}, z_{mp}, b_m, \gamma, \theta_{ijm}\}$, $m = 1, 2, \dots, M$, by fitting the TVCTF $H_{ij}(f'_q, t_p)$ of the channel model introduced in (1) as closely as possible to the TVCTF $\hat{H}_{ij}(f'_q, t_p)$ of the received RF signals. To compute the set \mathcal{P}_{t_p} , we chose the Euclidean norm as objective function $E(\mathcal{P}_{t_p})$, which measures the difference between the measured TVCTF $\hat{H}_{ij}(f'_q, t_p)$ and the TVCTF $H_{ij}(f'_q, t_p)$ of the channel model. In this regard, the objective function $E(\mathcal{P}_{t_p})$ is expressed as

$$E(\mathcal{P}_{t_p}) = \sum_{q=0}^{Q-1} \sum_{j=1}^{N_T} \sum_{i=1}^{N_R} |\hat{H}_{ij}(f'_q, t_p) - H_{ij}(f'_q, t_p)|^2. \quad (2)$$

$$h_{ijm_0}(f'_q, t_p) = \hat{H}_{ij}(f'_q, t_p) - \sum_{m=1, m \neq m_0}^M b_m^{(l)} [f_{ij}(x_{mp}, y_{mp}, z_{mp})]^{-\gamma/2} \exp\left(j\left(\theta_{ijm} - 2\pi(f'_q + f_c) \frac{g_{ij}(x_{mp}, y_{mp}, z_{mp})}{c_0}\right)\right) \quad (4)$$

$$\left(x_{m_0p}^{(l+1)}, y_{m_0p}^{(l+1)}, z_{m_0p}^{(l+1)}, b_{m_0}^{(l+1)}, \gamma^{(l+1)}, \theta_{ijm_0}^{(l+1)}\right) = \arg \min_{\mathcal{P}_{t_p}} \sum_{q=0}^{Q-1} \sum_{j=1}^{N_T} \sum_{i=1}^{N_R} \left| h_{ijm_0}(f'_q, t_p) - \frac{\exp\left(j\left(\theta_{ijm_0} - \frac{2\pi(f'_q + f_c)g_{ij}(x_{m_0p}, y_{m_0p}, z_{m_0p})}{c_0}\right)\right)}{b_{m_0}^{-1} [f_{ij}(x_{m_0p}, y_{m_0p}, z_{m_0p})]^{\gamma/2}} \right|^2 \quad (5)$$

$$b_{m_0}^{(l+1)} = \frac{\sum_{q=0}^{Q-1} \sum_{j=1}^{N_T} \sum_{i=1}^{N_R} [f_{ij}(x_{m_0p}^{(l)}, y_{m_0p}^{(l)}, z_{m_0p}^{(l)})]^{-\gamma(l)/2} \mathcal{R}\left\{\left(h_{ijm_0}(f'_q, t_p)\right)^* \exp\left(j\left(\theta_{ijm_0}^{(l)} - 2\pi(f'_q + f_c)g_{ij}(x_{m_0p}^{(l)}, y_{m_0p}^{(l)}, z_{m_0p}^{(l)})c_0^{-1}\right)\right)\right\}}{\sum_{q=0}^{Q-1} \sum_{j=1}^{N_T} \sum_{i=1}^{N_R} [f_{ij}(x_{m_0p}^{(l)}, y_{m_0p}^{(l)}, z_{m_0p}^{(l)})]^{-\gamma(l)}} \quad (6)$$

$$\left(x_{m_0p}^{(l+1)}, y_{m_0p}^{(l+1)}, z_{m_0p}^{(l+1)}, \gamma^{(l+1)}, \theta_{ijm_0}^{(l+1)}\right) = \arg \min_{\mathcal{P}_{t_p} \setminus \{b_{m_0}\}} \sum_{q=0}^{Q-1} \sum_{j=1}^{N_T} \sum_{i=1}^{N_R} \left| h_{ijm_0}(f'_q, t_p) - \frac{\exp\left(j\left(\theta_{ijm_0} - \frac{2\pi(f'_q + f_c)g_{ij}(x_{m_0p}, y_{m_0p}, z_{m_0p})}{c_0}\right)\right)}{(b_{m_0}^{(l+1)})^{-1} [f_{ij}(x_{m_0p}, y_{m_0p}, z_{m_0p})]^{\gamma/2}} \right|^2 \quad (7)$$

The set of parameters \mathcal{P}_{t_p} is determined by minimizing the objective function $E(\mathcal{P}_{t_p})$ in (2), i.e.,

$$\mathcal{P}_{t_p} = \arg \min_{\mathcal{P}_{t_p}} \sum_{q=0}^{Q-1} \sum_{j=1}^{N_T} \sum_{i=1}^{N_R} |\hat{H}_{ij}(f'_q, t_p) - H_{ij}(f'_q, t_p)|^2. \quad (3)$$

We start by setting the number of moving scatterers to 1, i.e., $m_0 = 1$, and choose arbitrary initial values for the quantities $x_{m_0p}^{(0)}, y_{m_0p}^{(0)}, z_{m_0p}^{(0)}, b_{m_0}^{(0)}, \gamma^{(0)}$, and $\theta_{ijm_0}^{(0)}$. At each iteration $l, l = 1, 2, 3, \dots$, we define the error function $h_{ijm_0}(f'_q, t_p)$ corresponding to the m_0 th moving scatterer as in (4) [see the top of this page], where $f_{ij}(x_{m_0p}, y_{m_0p}, z_{m_0p}) = D_{ijm_0}^T(t_p) D_{ijm_0}^R(t_p)$ and $g_{ij}(x_{m_0p}, y_{m_0p}, z_{m_0p}) = D_{ijm_0}^T(t_p) + D_{ijm_0}^R(t_p)$. The new estimates of the parameters $x_{m_0p}^{(l+1)}, y_{m_0p}^{(l+1)}, z_{m_0p}^{(l+1)}, b_{m_0}^{(l+1)}, \gamma^{(l+1)}$, and $\theta_{ijm_0}^{(l+1)}$, at every iteration $l, l = 0, 1, 2, \dots$, are computed according to the optimization problem in (5). Deriving the right-hand side of (5) w.r.t. the variable b_{m_0} and expressing the real part of a complex number by using the complex conjugation yield the exact closed-form solution to the new estimate of $b_{m_0}^{(l+1)}$ in (6) [see the top of this page], where $(\cdot)^*$ denotes the complex conjugate operator, and $\mathcal{R}\{\cdot\}$ refers to the real value operator. Replacing the new value of $b_{m_0}^{(l+1)}$ in (6) results in the new optimization problem as given in (7) [see the top of this page]. The new estimates of the remaining parameters, i.e., $x_{m_0p}^{(l+1)}, y_{m_0p}^{(l+1)}, z_{m_0p}^{(l+1)}, \theta_{ijm_0}^{(l+1)}$, and $\gamma^{(l+1)}$, are numerically determined by minimizing the right-hand side of (7) [see the top of this page]. For a fixed value of m_0 , the steps in (5)–(7) proceed until the relative error $E_{m_0}^{(l)}$ in the objective function $E(\mathcal{P}_{t_p})$ w.r.t. the number of iterations l is smaller than or equal to a predefined error level ε_1 . When this condition is met, the number of moving scatterers m_0 is increased by 1, i.e., $m_0 \leftarrow m_0 + 1$. Utilising the error function in (4) for the new value of m_0 and following the steps (4)–(7) allows the computation of the new estimates of $x_{m_0p}^{(l+1)}, y_{m_0p}^{(l+1)}, z_{m_0p}^{(l+1)}, b_{m_0}^{(l+1)}, \gamma^{(l+1)}$, and $\theta_{ijm_0}^{(l+1)}$ for the new value of m_0 . The proposed iterative positioning technique is repeated until no further progress can be made. In this case, the relative error E_{m_0} in $E(\mathcal{P}_{t_p})$ w.r.t. the number of moving scatterers m_0 is smaller than or equal to a predefined error level ε_2 , or a predetermined maximum M_{\max} is reached. As a result of the estimation method described in (4)–(7), we obtain the TV positions $(x_{m_0}(t), y_{m_0}(t), z_{m_0}(t))$ of the scatterer $S_{m_0}^M$.

Algorithm 1 describes the pseudo-code of the proposed

positioning method. Since this method requires extensive numerical computation, it is worthy to study its time complexity C_p . Assuming that the quantities N_T, N_R , and Q are constant, it can be concluded from Algorithm 1 that the complexity C_p of the estimation algorithm at the time instant t_p depends on the estimated number M of moving scatterers and the number L_{m_0} of interactions performed for each point scatterer $S_{m_0}^M, m_0 = 1, 2, \dots, M$ and $M \leq M_{\max}$. Based on [18, Section 4.1], we obtain the time complexity $C_p = \mathcal{O}(\sum_{m_0=1}^M L_{m_0})$, where $\mathcal{O}(\cdot)$ denotes the big- \mathcal{O} notation. Since the channel is non-stationary, the procedure is repeated at any time instant t_p .

Special cases: If the person is not moving then the proposed method simplifies to that described in [19]. For the case of WSS channels, where the speed of the person is constant during the observation time, the proposed positioning method reduces to the traditional INLSA algorithm [11], which has the same time complexity as the proposed algorithm for the entire observation time. A comparative analysis of the performance of the original INLSA procedure with alternative algorithms, e.g., ESPRIT¹ and SAGE², was conducted in [20].

IV. NUMERICAL RESULTS

In this section, the validation of the proposed iterative estimation procedure is performed by comparing the exact TV positions of the M moving scatterers S_m^M (body segments making up the human body) with the corresponding estimated TV positions. For a meaningful performance evaluation, one requires the prior knowledge of the exact TV coordinates $x_m(t_p), y_m(t_p)$, and $z_m(t_p)$ of the body segment modelled by the moving scatterer S_m^M . As is discussed in [21], existing IPSs do not provide ground truth information of the moving person. Their output is an estimation of the TV position of the person. To obtain the ground truth information for accurate evaluation of the algorithm's performance, we consider computer-simulated test RF signals with known TV positions.

As it was discussed in Section I, existing parameter estimation methods, which were developed in the context of wireless communications, assume that the channel is WSS and their generalization to non-stationary channels is not straightforward. Moreover, existing IPSs assume that the person is not

¹Estimation of signal parameters via rotational invariant techniques

²Space-alternating generalized expectation-maximization

Algorithm 1 Tracing of the body segments of a moving person at the time instant t_p

1: **Input:** $M_{\max} \in \mathbb{N}^*$, $\varepsilon_1 > 0$, $\varepsilon_2 > 0$, and a $Q \times P$ matrix containing the values of the TVCTF $H_{ij}(f_q, t_p)$
Output: Estimates of $P_{t_p} = \{x_{mp}, y_{mp}, z_{mp}, b_m, \gamma, \theta_{ijm}\}$

2: $m_0 \leftarrow 1$
3: **While** $m_0 \leq M_{\max}$ **or** $E_{m_0} > \varepsilon_2$
4: $l \leftarrow 0$
5: Define $x_{m_0p}^{(0)}$, $y_{m_0p}^{(0)}$, $z_{m_0p}^{(0)}$, $b_{m_0}^{(0)}$, $\gamma^{(0)}$, and $\theta_{ijm_0}^{(0)}$
6: Define $h_{ijm_0}^{(l)}(f'_q, t_p)$ according to (4)
7: **While** $E_{m_0}^{(l)} > \varepsilon_1$
8: Define the optimization problem as in (5)
9: Compute the new estimate of $b_{m_0}^{(l+1)}$ as in (6)
10: Update the optimization problem as in (7)
11: Compute the remaining parameters numerically
12: Update the optimization problem in (6)
13: $l \leftarrow l + 1$
14: Update the relative error $E_{m_0}^{(l)}$
15: **End**
16: $m_0 \leftarrow m_0 + 1$
17: Update the relative error E_{m_0}
18: **End**

moving for short time intervals in the order of a few seconds. Consequently, existing IPSs estimate the average positions and not the instantaneous positions [1], [8]. In addition, as is discussed in [9], the performance of existing positioning approaches is usually evaluated in customized and highly controlled settings, which are difficult to replicate. Because of these three limitations of existing methods no fair performance comparison with the proposed technique can be performed.

For the numerical validation of the proposed algorithm, we consider a room equipped with a 3×3 MIMO communication system. By considering the centre of the room as the origin, the locations of the distributed fixed omnidirectional transmit and receive antennas A_1^T , A_2^T , A_3^T , A_1^R , A_2^R , and A_3^R are $(-4.9, -2.4, -1.1)$, $(-4.9, -2.4, 1.1)$, $(-4.9, 2.4, 1.1)$, $(4.9, -2.4, -1.1)$, $(4.9, -2.4, 1.1)$, and $(4.9, 2.4, -1.1)$, respectively. For a realistic analysis, the simulation parameters were chosen in accordance with the IEEE 802.11n standard [13]. In this regard, the T_X and the R_X of the OFDM communication system are operating at $f_c=5.32$ GHz with a bandwidth $B = 20$ MHz. Although, the 802.11n standard considers the use of 30 sub-carriers, we select 1 out of 3 subsequent subcarriers to reduce the impact of noise. Therefore, we consider for our simulated signals $Q = 10$ subcarriers with $\Delta f'=1250$ kHz. The observation time T is 6 s with a sampling interval Δt of 0.01 s. The path loss component γ was set to 1.7. The positions of the $K_{ij} = 10$ fixed scatterers are generated randomly. A high-pass filter is employed to mitigate their contribution. The noise is modelled by a Gaussian random variable.

In the following, the human body is modelled by a cluster of $M = 13$ scatterers, which represent the centres of mass of the humeri (upper arm bones), radii (lower arm bones), femurs (thigh bones), tibias (largest lower leg bones), hands, toes, and pelvis/torso. For realistic trajectories $x_m(t)$, $y_m(t)$, and $z_m(t)$ of the centre of mass of the m th body segment S_m^M , we employ the OpenSim workflow [12], which has a broad range of capabilities for generating and analyzing the dynamics of a system of rigid bodies and joints that are acted upon by forces

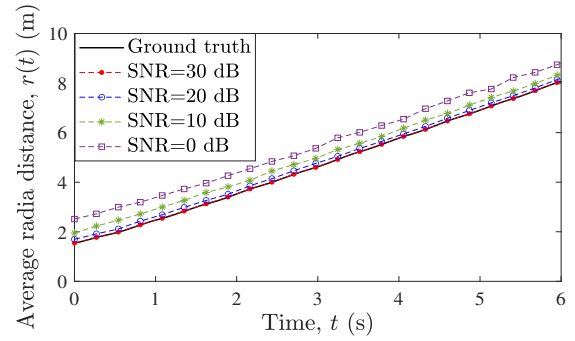


Fig. 2. Impact of noise on the estimation of the average radial distance $r(t)$.

to produce motion. Here, the input of the OpenSim tool is the validated full-body musculoskeletal model published in [22].

For this scenario, Fig. 2 presents a comparison of the ground truth of the average radial distance $r(t) = [\sum_{m=1}^M \sqrt{x_m^2(t) + y_m^2(t) + z_m^2(t)}] / M$ with the corresponding estimation results for different values of the SNR and 30 trials. As can be observed, the accuracy of the estimation procedure decreases with decreasing values of the SNR. However, this observation does not apply to a specific time t_p . To quantitatively evaluate the average estimation error of the proposed iterative method, we present the absolute average error of the displacements $x_m(t)$, $y_m(t)$, and $z_m(t)$ ($m = 1, 2, \dots, M$) in Table I. This table also presents the impact on the absolute average errors of the TV speed and the TV Doppler frequencies for different values of the SNR. The Doppler frequencies $f_{ijm}(t)$ are obtained as $f_{ijm}(t) = -2\pi(f'_q + f_c)\dot{\tau}'_{ijm}(t)$, where $\dot{\tau}'_{ijm}(t)$ is the time derivative of the TV path delay $\tau'_{ijm}(t)$ at time t , which can be expressed in terms of the TV coordinates $x_m(t)$, $y_m(t)$, and $z_m(t)$ of the moving scatterers S_m^M . For completeness, we also present in Table I the absolute average errors of the TV mean Doppler shift and the TV Doppler spread, the expressions of which can be found in [23, Eqs. (21) and (23)]. The performance of the proposed positioning method is analyzed for different values of the SNR ranging from 0 dB to infinity (no noise). SNR values between 0 dB and 10 dB describe scenarios where the moving person is far from or out of the range of the communication system. All estimation results in Table I are computed by averaging over the $M = 13$ moving point scatterers, the observation time $T = 6$ s, the subcarriers $Q = 10$, and 30 trials. Here, we average over 30 trials to mitigate the impact of the random phases θ_{ijm} as well to fairly assess the impact of the noise. As can be observed from Table I, the accuracy of the estimation algorithm decreases with decreasing values of the SNR. The second column of Table I shows that for SNR values strictly larger than 15 dB the proposed algorithm can locate the person with an average absolute estimation percentage error of less than 2.5%. Here, the percentage error is computed as the difference between the ground truth (known) value and the estimated value, divided by the ground truth value and multiplied by 100. For SNR values around 10 dB, the average absolute error is approximately 7.80%. Columns three and four of Table I show that the TV speed and TV Doppler frequency behave similarly with respect to noise, especially for SNR values higher than 15 dB, for which the absolute estimation error is less or equal to 5%. In the case where the SNR is less or equal to 10 dB,

TABLE I
AVERAGE ABSOLUTE ESTIMATION ERROR FOR DIFFERENT VALUES OF THE SNR

SNR in dB	TV displacement		TV speed		TV Doppler frequency		TV mean Doppler shift		TV Doppler spread	
	in m	%*	in m/s	%*	in Hz	%*	in Hz	%*	in Hz	%*
∞ (no noise)	0.015	0.29	0.013	0.95	0.142	2.75	0.129	4.17	2.01	7.27
25	0.021	0.43	0.017	1.25	0.18	3.48	0.150	4.85	21.7	97.17
20	0.032	0.65	0.024	3.26	0.258	5.00	0.308	9.96	45.6	165.15
15	0.120	2.46	0.038	5.16	0.52	10.09	0.516	16.69	101.2	365.80
10	0.380	7.80	0.314	23.08	2.081	40.40	2.135	69.09	213.3	772.54
5	0.532	10.92	0.624	45.80	4.804	93.28	5.386	174.30	340.2	1231.43
0	0.890	18.27	0.935	68.70	9.672	187.80	8.187	264.95	451.9	1636.72

* The symbol % refers to the percentage error.

the estimation accuracy degrades considerably. Now, the fifth column of Table I illustrates the fact that the TV Doppler spread is more sensitive to noise than the TV mean Doppler shift because it is impacted by the average absolute error of the Doppler frequencies as well as by the average absolute error of the TV path gains $c_{ijm}(t)$. This behavior is more pronounced in the TV Doppler spread. The last column of Table I clearly shows that the TV Doppler spread is sensitive to small variations of the TV displacements $x_m(t)$, $y_m(t)$, and $z_m(t)$. In fact, even in the absence of noise (SNR $\rightarrow \infty$), an average absolute displacement error of approximately 1.5 cm (0.29 %) results in an average absolute Doppler spread error of approximately 2.01 Hz (7.27 %). This could explain why the TV Doppler spread has not been used for determining the TV positions of moving persons in indoor environments. This analysis of the effects of positioning errors on micro-Doppler human signatures is of great interest for optimal selection of classification metrics of future RF-sensing applications.

V. CONCLUSION

A new iterative method to trace the body segments of a moving person leveraging RF signals in non-stationary indoor areas has been proposed in this paper. Each segment of the human body acts as a relay and is modelled by a moving point scatterer. The introduced algorithm uses MIMO techniques and estimates the TV positions of the moving scatterers by fitting the TVCTF of the received radio signals as close as possible to the TVCTF of the 3D non-stationary channel model. Numerical results were provided to evaluate the performance of the positioning method for various values of the SNR. On average, it was shown that our procedure estimates the TV positions with an accuracy higher than 92 % for SNR values larger or equal to 10 dB.

REFERENCES

- [1] A. Yassin et al., "Recent advances in indoor localization: A survey on theoretical approaches and applications," *IEEE Commun. Surveys & Tuts.*, vol. 19, no. 2, pp. 1327–1346, 2nd Quart. 2017.
- [2] M. U. Ali, S. Hur, S. Park, and Y. Park, "Harvesting indoor positioning accuracy by exploring multiple features from received signal strength vector," *IEEE Access*, vol. 7, pp. 52110–52121, Apr. 2019.
- [3] Y. Lin, Y. Chiou, and T. Lin, "Geometric positioning techniques based on tracking algorithm for indoor dynamic environments," in *Int. Conf. on Advanced Manuf. (ICAM'18)*, Yunlin, Taiwan, Nov. 2018, pp. 131–133.
- [4] J. Wang et al., "Low human-effort, device-free localization with fine-grained subcarrier information," *IEEE Trans. Mobile Computing*, vol. 17, no. 11, pp. 2550–2563, Nov. 2018.
- [5] Y. Tao and L. Zhao, "A novel system for WiFi radio map automatic adaptation and indoor positioning," *IEEE Trans. Veh. Technol.*, vol. 67, no. 11, pp. 10683–10692, Nov. 2018.
- [6] X. Niu, T. Liu, J. Kuang, and Y. Li, "A novel position and orientation system for pedestrian indoor mobile mapping system," *IEEE Sensors J.*, vol. 21, no. 2, pp. 2104–2114, Jan. 2021.
- [7] A. Correa, M. Barcelo, A. Morell, and J. L. Vicario, "A review of pedestrian indoor positioning systems for mass market applications," *Sensors*, vol. 17, no. 8, pp. 1927, 2017.
- [8] R. F. Brena et al., "Evolution of indoor positioning technologies: A survey," *J. of Sensors*, Mar. 2017.
- [9] R. Montoliu, E. Sansano, J. Torres-Sospedra, and O. Belmonte, "Indoorloc platform: A public repository for comparing and evaluating indoor positioning systems," in *Int. Conf. on Indoor Position. and Indoor Navigation (IPIN'17)*, Sapporo, Japan, Sept. 2017, pp. 1–8.
- [10] K. Qian et al., "Widar2.0: Passive human tracking with a single Wi-Fi link," in *16th Annual Int. Conf. on Mobile Syst., Appl., and Services (MobiSys'18)*, Munich, Germany, Jun. 2018, pp. 350–361.
- [11] D. Umansky and M. Pätzold, "Design of measurement-based wideband mobile radio channel simulators," in *4th Int. Symp. on Wireless Commun. Syst. (ISWCS'07)*, Trondheim, Norway, Oct. 2007, pp. 229–235.
- [12] J. Hicks, "OpenSim documentation," Available: <https://simtk-confluence.stanford.edu/x/pga9AQ>, 2018.
- [13] "IEEE Standard for Information technology– Local and metropolitan area networks– Specific requirements– Part 11: Wireless LAN Medium Access Control (MAC) and Physical Layer (PHY) Specifications Amendment 5: Enhancements for Higher Throughput," *IEEE Std 802.11be-2019*, pp. 1–565, Piscataway, NJ, USA, 2009.
- [14] National Research Council (US) et al., "Effects of electromagnetic fields on organs and tissues," in *Assess. of the Possible Health Effects of Ground Wave Emergency Net.* National Academies Press (US), 1993.
- [15] N. Golestani and M. Moghaddam, "Theoretical modeling and analysis of magnetic induction communication in wireless body area networks (WBANs)," *IEEE J. of Electromagnetics, RF, and Microwaves in Medicine and Biology*, vol. 2, no. 1, pp. 48–55, Feb. 2018.
- [16] A. Abdelgawwad, A. Borhani, and M. Pätzold, "Modelling, analysis, and simulation of the micro-Doppler effect in wideband indoor channels with confirmation through pendulum experiments," *Sensors*, vol. 20, no. 4, pp. 1049, 2020.
- [17] A. Abdelgawwad, A. Catala, and M. Pätzold, "Doppler power characteristics obtained from calibrated channel state information for human activity recognition," in *91st Veh. Technol. Conf. (VTC'20-Spring)*, Antwerp, Belgium, May 2020, pp. 1–7.
- [18] S. Dasgupta, C. H. Papadimitriou, and U. V. Vazirani, *Algorithms*, McGraw-Hill Higher Education New York, 2008.
- [19] R. Hicheri and M. Pätzold, "A new iterative estimation procedure for the localization of passive stationary objects from received RF signals in indoor environments," in *90th Veh. Technol. Conf. (VTC'19-Fall)*, Honolulu, Hawaii, USA, Sept. 2019, pp. 1–6.
- [20] A. Fayziyev and M. Pätzold, "The performance of the INLSA in comparison with the ESPRIT and SAGE algorithms," in *Int. Conf. on Advanced Technol. for Commun. (ATC'14)*, Hanoi, Vietnam, Oct. 2014, pp. 332–337.
- [21] Martínez de la Osa et al., "Positioning evaluation and ground truth definition for real life use cases," in *7th Int. Conf. on Indoor Positioning and Indoor Navigation (IPIN'16)*, Madrid, Spain, Oct. 2016.
- [22] A. Rajagopal et al., "Full-body musculoskeletal model for muscle-driven simulation of human gait," *IEEE Trans. Biomed. Eng.*, vol. 63, no. 10, pp. 2068–2079, 2016.
- [23] A. Borhani and M. Pätzold, "A non-stationary channel model for the development of non-wearable radio fall detection systems," *IEEE Trans. Wireless Commun.*, vol. 17, no. 11, pp. 7718–7730, Sept. 2018.